Accepted manuscript doi:
10.1680/jgeot.18.p.005

Submitted: 06 January 2018

Published online in 'accepted manuscript' format: 25 September 2018

Manuscript title: Evolution of bulk compressibility and permeability of granite due to thermal cracking

Authors: Fan Zhang*[†], Jianjian Zhao*, Dawei Hu[†], Jianfu Shao*[‡] and Qian Sheng[†]

Affiliations: *School of Civil Engineering, Architecture and Environment, Hubei University of Technology, Wuhan 430068, China; [†]State Key Laboratory of Geomechanics and Geotechnical Engineering, Institute of Rock and Soil Mechanics, Chinese Academy of Sciences, Wuhan Hubei 430071, China and [‡]University of Lille, Laboratory of Multi-scale and Multi-physics Mechanics (Lamcube), Villeneuve d'Ascq, France

Corresponding author: Jianfu Shao, School of Civil Engineering, Architecture and Environment, Hubei University of Technology, Wuhan 430068, China; University of Lille, Laboratory of Multi-scale and Multi-physics Mechanics (Lamcube), Villeneuve d'Ascq, France.

E-mail: jian-fu.shao@polytech-lille.fr

Accepted manuscript doi:
10.1680/jgeot.18.p.005

Abstract

Granite samples were subjected to heating at different temperatures and rapid water cooling. Hydrostatic compression tests were performed on the thermally treated samples. The initial tangent bulk modulus was measured. The critical value of hydrostatic stress for closing thermally induced micro-cracks was identified and the residual volumetric strain after unloading was determined. Gas permeability of granite samples was also determined under different levels of hydrostatic stress. It is found that the density of thermally induced micro-cracks can be correlated with the residual volumetric strain, both increasing when the pre-treatment temperature is higher. There is a significant increase of gas permeability up to several orders of magnitude as a consequence of micro-cracks induced by the heating and water cooling process.

Keywords: Granite; heating; cooling; cracking; permeability; bulk compressibility

Accepted manuscript doi:
10.1680/jgeot.18.p.005

1. Introduction

Hot Dry Rock (HDR) resources, exploited as heat from rocks with a temperature in the range of 150^{o}C to 650^{o}C and at about 3 to 5 kilometers below the earth's surface, have attracted much attention during the recent years. HDR resources, unlike coal, oil and other traditional resources that produce a lot of carbon dioxide emission and other environmental pollutions, is one of the environmental-friendly green resources. In addition, according to previous studies (Bruel 2007, Gnatus and Khutorskoy 2010, Zeng et al. 2013, Chen and Jiang 2015, Kelkar et al. 2015), there is huge HDR resources distributed in different countries around the word. HDR resources are commonly used for heating or power generation. For instance, the basic procedure of exploiting HDR resources is composed of following steps (Abbasi et al. 2017, Tomac and Sauter 2017). At the first step, the cold ground water is injected into the HDR formation through injection wells to capture heat energy. During the second step, the obtained hot water or vapor is extracted out of the ground through production wells to generate power. Finally, the cooled water is pumped back to the injection wells to achieve the recycling of resources.

In this context, hot rocks are experiencing a rapid water-cooling treatment under high temperatures. This can induce significant changes in mechanical and physical properties of rocks and represent a potential risk to the long-term stability of HDR exploitation facilities (Wnuk 1982, Berthomieu and Jouanna 1984, Boukharov et al. 1995, Zhao et al. 2015). Laboratory tests on deformation of borehole at high temperature and high pressure indicated

that borehole approached the critical condition when the temperature is between 400^{o}C and 500^{o}C (Zhao et al. 2015). The physical properties, for instance permeability, ultrasonic wave and thermal conductivity, of granite samples after temperature pre-treatment have been investigated in a number of previous studies (Yong and Wang 1980, David et al. 1999, Chaki et al. 2008, Yavuz et al. 2010, Brotons et al. 2013, Gaunt et al. 2016, Chen et al. 2017, Violay et al. 2017). Most studies have shown similar trends on evolutions of physical and mechanical properties with increasing temperature. The physical and mechanical properties of granite are nearly unchanged when the heating temperature is below 300^{o}C, and show a small variation for the temperature ranging from 300^{o}C to 500^{o}C. The thermal weakening effect becomes more pronounced when the temperature exceeds about 500^{o}C. Microscopic observations have also been conducted and it is found that the degradation in physical and mechanical properties is directly related to the heating induced microcracks (Fredrich and Wong 1986, David et al. 1999, Chaki et al. 2008, Yavuz et al. 2010, Brotons et al. 2013, Gaunt et al. 2016, Chen et al. 2017, Griffiths et al. 2017). Similar results have been reported in other studies on granite and other kinds of rocks (Heuze 1983, Zhang et al. 2009, Chen et al. 2012, Shao et al. 2015, Tian et al. 2016, Zhao 2016, Huang et al. 2017, Yang et al. 2017). A number of previous studies (Yavuz et al. 2010, Gaunt et al. 2016, Zhang et al. 2018) have tried to provide some microscopic explanations on the degradation of both physical and mechanical properties of granite caused by heating treatment. The granite is a medium constituted of solid particles and bonded interfaces between particles. The thermal stress during heating treatment may induce

the de-bonding of interfaces between particles. In addition, the growth of heating induced cracks can be influenced by solid particle size (Shao et al. 2014, Zhang et al. 2018).

A number of previous studies have focused on mechanisms of generation and growth of thermal microcracks. For instance, according to (Manson and Smith 1955), the failure of many brittle materials depends upon the stress distribution rather than the maximum stress. In other studies (Hasselman 1963, Hasselman 1969, Fredrich and Wong 1986), the crack propagation in brittle ceramics subjected to thermal shock has been studies. It is found that the driving force for crack propagation is provided by the elastic stored energy and the thermal stress induced crack instability occurs between two values of critical crack length. Johnston and Toksoz (Johnston and Toksoz 1980) have defined the threshold temperature and introduced a parameter to investigate the role of crack and grain boundary contacts in determining seismic wave attenuation in rock. Kawai and Yamakawa (Kawai and Yamakawa 1997) have investigated the effect of microstructure on the flexural strength. More recently, Griffiths et al. (2018) have investigated the thermal microcracking in Westerly Granite using direct wave velocity, coda wave interferometry and acoustic emissions.

Furthermore, the effects of cooling rate on mechanical properties of rocks were also analyzed. According to (Zhang et al. 2017), the thermal damage is highly dependent on the cooling method. The samples subjected to a rapid cooling process can exhibit a considerably higher thermal crack density than those subjected to a slow cooling process (Shao et al. 2014, Kumari et al. 2017). The thermomechanical responses of water-saturated limestone during

thermal cycles under constant hydrostatic and deviatoric stresses were analyzed (Pei et al. 2016). It is found that the applied stress level can intensify the thermal damage.

In spite of existing studies, the physical and mechanical properties of thermally pre-treated granite under high hydrostatic stresses need still be investigated. This feature is important for the stability assessment of borehole in HDR exploitation facilities and will be investigated in the present study. Compared with existing studies, several new features are considered in the present study. The samples are subjected to shock cooling and we try to verify whether the rapid cooling would add complementary damage is the thermally cracked granite samples. On the other hand, hydrostatic tests are performed until different values of confining pressure to identify the progressive closure of thermally induced cracks. It is of concern here to investigate that beyond a certain confining pressure, the effect of thermal micro-cracking on mechanical properties becomes neglected, in contrast to the case of uniaxial compression.

2. Material description and experimental procedure

2.1 Material description and samples preparation

The material tested is granite. Large granite blocks were collected from Dabie mountains area of Hubei Province, China. Cylindrical samples were then drilled from the large blocks without apparent cracks. The petro-physical analysis with the X-ray diffraction technique (XRD) has been realized (Zhang et al., 2018) and showed that the granite was mainly composed of feldspar, mica and quartz. The average mass percentages of different mineral phases were respectively 21.05% for albite, 45.19% for potash feldspar, 23.19% for mica and 8.87% for

quartz. Some secondly minerals were also found such as calcite and chlorite-serpentine with a volumetric fraction of about 1.28%. The water porosity measurement method has also been described in Zhang et al. (2018). The average porosity of the granite was 1.82% and the natural density was 2.61 g/cm^3.

The size of cylinder samples for hydrostatic compression tests is 50 mm in diameter and 100 mm in length. All the samples are checked in accordance with the standard requirements of the International Society of Rock Mechanics (ISRM 1979), in particular with the parallelism within ±0.05 mm and the surface flatness within ±0.02 mm. The granite samples are first subjected to a heating and rapid cooling treatment. Hydrostatic compression tests and gas permeability tests are then carried out on the thermally treated samples. A detailed description of thermal treatment and experimental procedure is provided below.

2.2 Thermal treatment

Six levels of pre-treatment temperature are selected such as 200, 300, 400, 500, 600 and 900^{o}C. The samples are heated in a furnace at atmospheric pressure with a rate of 5^{o}C/min until a selected value. The samples are maintained at the selected temperature for a period of stabilization of four hours. The heating rate used is considered as low enough in order to avoid a high thermal gradient and the stabilization period is used to obtain a uniform distribution of temperature inside samples. According to the previous study (Zhang et al., 2018), the thermal conductivity of intact granite sample is equal to 2.65W/(m·K). A preliminary thermal conductivity calculation was done using the given size of sample, the specific heat capacity of

granite (920J/(kg.K)) and the density of sample (2.61 g/cm^3). If the sample's initial temperature is equal to the 25°C and it is subjected to a heating temperature of 900°C, it should take about 1.75h so that the temperature inside the whole sample reaches the desired value for the sample size used here. Therefore, the heating stabilization period of four hours used in the present study seems to be reasonable. The heated samples are then rapidly cooled by water immersion in a container with a volume of 25 liters at room temperature during one hour. The rate of cooling in the water is not easy to control. The temperature of samples is monitored by the thermocouple that is attached to the surface of samples. The monitor shows that the temperature drop from 900^{o}C to room temperature takes about 48 minutes. Therefore it is decided to keep the sample in water for one hour. Finally, the samples are kept inside a desiccator until the completion of subsequent tests. The weight of samples is regularly measured using a balance with a precision of 0.01g. When the weight variation is less than 0.01% during a week, the sample is considered as fully dried.

2.3 Testing apparatus

The hydrostatic compression tests were conducted under drained conditions using a home-designed testing system. A schematic illustration of the testing system is shown in Fig. 1, mainly including the confining pressure chamber, the axial force cylinder and the counterforce frame. The hydrostatic stress is generated by hydraulic oil injected by an electro-hydraulic servo pump. The maximum designed pressure is 60MPa. The axial strain and radial strains of the samples are measured by four strain gauges (two in each direction). The axial force is

measured by an internal transducer in order to reduce the friction on the axial force piston. The home-designed gas permeability device is shown in Fig. 2. This device is especially designed for the measurement of a large range of permeability from 10^{-12} m^2 to 10^{-22} m^2. The principle of the device is to generate a continuous gas flow through the tested sample under a steady flow condition. Gas is injected into the sample with a constant inlet pressure from the buffer reservoir while the atmospheric pressure is prescribed at the outlet side of sample. The testing system contains a high-precision electro-hydraulic servo pump and it can ensure the stability of applied stress while measuring deformation and permeability. The strain measurement is performed continuously throughout the test and the permeability measurement is performed when the stress reaches a steady state.

2.4 Hydrostatic compression test procedure

Hydrostatic compression tests are performed on heating-cooling treated granite samples under a constant temperature of about 20±2°C. The hydrostatic stress is generated by applying a confining pressure to the tested cylinder sample. The sample is isolated by a high-strength rubber jacket. The top and bottom ends of the jacket are fixed with steel clamps to the up and down pistons of pressure chamber. Each test is conducted in three steps. The sample is first placed into the confining pressure chamber. The pressure chamber is then filled with hydraulic oil and the exhaust valve is closed after the air bubbles are completely removed. The confining pressure is finally increased by the injection of oil into the closed chamber with a prescribed rate of 7×10^{-2} MPa/s in drained condition without pore fluid pressure. According to

preliminary studies, this load rate is considered as small enough to avoid over pore pressure generated by the hydrostatic stress. In order to reduce experimental scatters, for each value of pre-heating temperature, three hydrostatic compression tests are realized on three different samples subjected to the same pre-heating temperature and the average values of strains are calculated and presented.

2.5 Gas permeability testing procedure

Permeability evolution in rocks is generally related to growth of microcracks. In the present study, the permeability evolution is used as a parameter to characterize the thermally induced microcracks. The initial permeability of granite is generally very small. Even with the heating-cooling induced microcracks, the average permeability of granite samples still remains small. The measure of water permeability takes a longer time than that of gas permeability. Therefore, the gas permeability is preferred in the present study. Further, as shown in previous studies (Tanikawa and Shimamoto 2006, Picandet et al. 2009, Ougier-Simonin et al. 2011), the use of gas as flow fluid can more accurately capture a wide range of permeability than water.

The jacketed granite sample is subjected to a constant confining pressure of 5 MPa, which is applied to prevent the gas flow through the interface between the jacket and sample. The steady flow method is used for the measurement of gas permeability and the argon gas with a purity of 99% is chosen as the injection fluid. The permeability test is composed of the following steps (Loosveldt et al. 2002).

The argon gas is injected from the buffer reservoir which is supplied with gas by an external source. The valve connected to the external source is closed once the pressure in the buffer reservoir is increased up to the selected value $P_1 = 1.5MPa$.

The gas continuously flows from the bottom surface to upper side of the sample which is at the atmospheric pressure P_0. This generates a drop of pressure in the buffer reservoir ΔP_1, which is limited to a low value of 0.1 MPa during the injection time Δt. Thereafter, it is assumed that a steady-state flow regime is established in the sample at the constant mean injection pressure calculated by $P_m = P_1 - (\Delta P_1/2)$.

The mean volume flow rate Q_m is calculated by $Q_m = \Delta\rho V_r/\rho\Delta t$ where V_r is the volume of the buffer reservoir and the pipes connected to the sample, $\Delta\rho$ is the variation of the gas specific mass due to ΔP_1. We assume that the argon is an ideal gas and the test is performed under an isothermal condition. Therefore, the mean volume flow can be calculated by $Q_m = V_r \Delta P_1/\Delta t P_m$. Finally, the overall permeability of the sample (K) is calculated by using Darcy's law and by taking into account the Klinkenberg effect (Loosveldt et al. 2002) using the following relation:

$$K = \frac{\mu Q_m}{S} \frac{2hP_m}{\left(P_1^2 - P_0^2\right)} \qquad (1)$$

where μ, S and h respectively denote the gas viscosity, the cross-section and height of the sample.

Accepted manuscript doi:
10.1680/jgeot.18.p.005

3. Experimental results

3.1. Cracks induced by heating-cooling treatment

The thermal treatment induces a change in the sample surface color as shown in Fig. 3. The surface color of damaged samples is lighter than that of the intact one. The change is moderate when the pre-treatment temperature is below 400°C. But the change becomes significant when the pre-treatment temperature is higher than 500^{o}C. On the other hand, in order to show the cracking of granite samples by the heat-cooling treatment, the polarized light microscopy images are obtained and presented in Fig. 4. The magnification of images is 10 times. In Fig. 5, we show the scanning electron microscope (SEM) images of the sound sample and the samples subjected to the different levels of heating-cooling temperature. Very few initial microcracks are observed in the sound sample (Fig. 5a). A small number of microcracks with small width and length are generated on weak surfaces of crystals in the sample heated up to 200^{o}C (Fig. 5b). With the increase of temperature, there is a significant increase in crack number, width and length (Figs. 5d to 5e). Some cracks start to connect each other and those around crystals become bumpy. When the pre-hating treatment temperature is below 500^{o}C, the thermal cracks essentially occur around grains. When the temperature exceeds 500^{o}C, the thermal cracks are generated in a large quantity.

3.2. Bulk compressibility and crack closure stress

The evolution of bulk compressibility of granite due to heating-cooling induced microcracks is here characterized from volumetric strains obtained in hydrostatic compression tests. As mentioned above, a series of hydrostatic compression tests are performed up to a confining pressure of 50 MPa on samples with different values of pre-heating temperature. The typical stress-strain curves (averaged from three different tests) are presented in Fig. 6. For the sound sample without pre-heating treatment, the radial strain is almost identical to the axial one. This indicates that the sound granite sample has an isotropic behavior. However, in the samples subjected to the heating-cooling treatment, the axial strain is larger than the radial one. For instance, at the hydrostatic stress of 50 MPa, the axial strain is approximately 1.5 times that of the radial strain. In order to establish some correlations between thermal cracks and macroscopic volumetric strains, the volumetric strains are calculated by $\varepsilon_v = \varepsilon_a + 2\varepsilon_r$, ε_a being the axial strain and ε_r the radial one. The obtained volumetric strains are presented in Fig. 7. For almost all levels of pre-treatment temperature, two distinct zones can be observed on the volumetric strain curve. In the first zone when the applied hydrostatic stress is smaller than a critical value, the volumetric strain exhibits a nonlinear concave behavior. The initial loading tangent modulus of the volumetric strain curve is generally used to characterize the initial elastic compressibility of cracked material before closure of microcracks. This modulus is here defined by the inclination of a tangent line at the origin of the volumetric strain curve and calculated by the following simplified from:

$$K_{\mathrm{i}} = (\sigma_{10} - \sigma_0)/(\varepsilon_{10} - \varepsilon_0) \qquad (2)$$

where K_{i} denotes the initial bulk modulus. σ_{10} and ε_{10} are the hydrostatic stress and volumetric strain corresponding to 10% of final value of confining stress. σ_0 and ε_0 are hydrostatic stress and volumetric strain corresponding to the starting loading point. A schematic illustration is presented in Fig. 6a. The obtained values are given in Table 1 and plotted in Fig. 8 for different values of pre-treatment temperature. The initial bulk modulus significantly decreases with the pre-treatment temperature due to the increase of crack density.

In the second zone, after most microcracks are progressively closed, a linear elastic response phase is recovered. The critical value of hydrostatic stress at the transition from the nonlinear to linear zones can be interpreted as the closure stress of microcracks. The closure stress is about 35 MPa and does not vary significantly when the pre-treatment temperature ranges from 25°C to 400°C, as shown in Figs. 8 and 9. However, the corresponding volumetric strain at the crack closure state continuously increases with the pre-treatment temperature due to the increase of thermal induced crack density. However, when the pre-treatment temperature is greater than 500°C, there is an important increase of crack closure stress. For instance, for the sample with pre-treatment temperature at 500°C, the crack closure stress approaches 50MPa. For the samples with pre-treatment temperature at 600°C and 900°C, it is even impossible to identify the crack closure stress until the maximum hydrostatic stress used in the test is reached. This means that for these two groups of granite samples, the crack closure stress should be higher than 50MPa. Therefore, it seems that for a given pre-heating temperature, it

will be possible to define a hydrostatic compressive stress threshold above that the heating-cooling process does not affect mechanical properties of granite. On the other hand, the residual volumetric strains after the elastic unloading of applied hydrostatic stress are also calculated and presented in Fig. 8 as functions of pre-treatment temperature. The residual strain significantly increases with the pre-treatment temperature.

3.3 Gas permeability

The gas permeability is here used as an indicator of cracking in granite samples treated by heating and water cooling process. It is measured at different values of hydrostatic stress. In Figs. 10 and 11, we show the gas permeability evolutions respectively with hydrostatic stress and pre-treatment temperature. One can see that the gas permeability continuously decreases with the applied hydrostatic stress. On the other hand, the gas permeability significantly increases with the pre-treatment temperature. Quantitatively, up to the pre-treatment temperature of 300°C, the gas permeability decrease due to hydrostatic compression is more important than the permeability increase due to heating-cooling process. However, when the pre-treatment temperature is higher than 400^{o}C, there is a sudden increase of gas permeability due to thermal treatment while the magnitude of permeability decrease due to hydrostatic compression remains nearly the same as that for lower pre-treatment temperatures. For example, under a hydrostatic stress of 50MPa, the gas permeability of sound samples is of the order of 10^{-18} m^2 and nearly remains unchanged until 400°C. But it is increased to the order of 10^{-16} m^2 at the pre-treatment temperature of 900^{o}C. This indicates that the thermally induced

crack density becomes very important so that the majority of microcracks are not closed by hydrostatic compression up to 50MPa.

4. Discussions of results

4.1. Analysis of cracking by heating-cooling treatment

The surface color change shown in Fig. 3 is probably related to the modification of minerals during the heating and water-cooling process. In order to show that the heating process can generate mineral composition changes inside granite, an X-Ray Diffraction test is performed. With the increase of pre-heating treatment temperature up to 900^{o}C, the content of quartz increases to 13.54%, the content of potash feldspar gradually decreases to 16.45%, and the chlorite gradually disappears. The chlorite shows a pale green color at low temperature (Hajpal and Torok 2004). The color of potash feldspar is usually a bit dark and that of quartz is a bit bright. According to (Beck et al. 2015), the color change of rocks can be due to the transformation of calcite. They found that the color of calcite changed from dark to white due to thermal treatment.

By comparing the polarized light microscopy images of the intact sample (Fig. 4a) and that corresponding to the heat temperature of 900^{o}C (Fig. 4b), one can see that a high number of microcracks are generated on the surface of the granite sample after the heating-cooling treatment. About the microcracks observed in Fig. 5, according to previous investigations (Glover et al. 1995, Nasseri et al. 2009), when the pre-treatment temperature reaches 600^{o}C, quartz generally undergoes the transition in crystal structure from α-type to β-type at 573^{o}C. A

number of trans-granular cracks are created and a number of crystals are divided into small pieces by the trans-granular cracks (Figs. 5f to 5g). Nasseri et al. (Nasseri et al. 2009) have also investigated thermal microcracks in granite by using SEM analysis and they have obtained similar results. Moreover, Mallet et al. (Mallet et al. 2013) have tried to provide a quantitative characterization of the density of thermal induced cracks in terms of crack length and number. In the present study, only a qualitative analysis is provided and the emphasis is put on the effect of thermal cracking on mechanical properties and permeability evolution of granite. However, the SEM images only provide a 2D description of thermal induced micro-cracks. In future studies, it will be interesting to investigate the 3D spatial distribution of induced micro-cracks. This can be done by using micro-tomography imaging or by measuring elastic wave velocity at different levels of the sample.

4.2. Thermal cracking induced anisotropy and residual strain

Anisotropic strains in hydrostatic compression tests are observed in the samples subjected to heating-cooling treatment. This is a new result compared with existing studies. Indeed, according to the study on heating induced cracks in two basalts (Etna basalts and Iceland basalts) reported in Vinciguerra et al. (2005), the thermal cracks exhibits essentially an isotropic distribution. The anisotropy of thermal cracks in granite observed in the present study seems to indicate that the distribution of heating-cooling induced cracks can be related to mineral compositions and microstructures of rocks as well as tested sample geometry. Indeed, the orientation of cracks around grains can be affected by the shape and orientation of grains.

Accepted manuscript doi:
10.1680/jgeot.18.p.005

Further, as a rapid cooling method is adopted in this study, a strong temperature gradient is created in the sample during the cooling period. The cooling-induced cracking process can be sensitive to kinematic constraints in the axial and radial directions of sample. As the length is twice of the diameter, the kinematic constraint in the axial direction is larger than the radial one. Therefore, we can assume that more cracks are induced in the radial direction than the axial one. Under the subsequent hydrostatic compression, more cracks are closed in the axial direction (cracks parallel to the radial axis) than in the radial one (cracks parallel to the axial axis). This leads to that the axial strain is larger than the radial one. Compared with other studies (Vinciguerra et al. 2005; Wang et al. 2013) where a slow cooling procedure was used and an isotropic distribution of thermal cracks was observed, the main difference of the present study is that a rapid cooling method is adopted. It seems that the anisotropy of thermal cracks can be related to the cooling procedure. However, a deeper microscopic analysis on the spatial distribution of cracks is needed to confirm this assumption.

The residual strains reported in Figs. 8 and 9 are an interesting feature of thermal microcracking process. Indeed, in hard rocks like granite, plastic deformation is generally negligible. The nucleation and propagation of microcracks is a main mechanism of inelastic dissipation and failure (Wong 1982; Zhu et al. 2016). Macroscopic irreversible residual strains are generally related to the friction sliding along microcracks at the microscopic scale. Therefore, in the present study, the residual strain is used as a macroscopic parameter to quantify the density of micro-cracks created by the heating and water cooling process. It is

clearly observed that the residual strain increases when the pre-treatment temperature is higher. For the samples with the pre-treatment temperature over 500°C, as the crack closure stress is higher than 50MPa, the elastic stage after the crack closure is not obtained. Therefore, the residual strain estimated at 50MPa is clearly an underestimation of the real value. Nevertheless, it seems that there is a sudden increase of residual strain and crack closure stress between 400°C and 500°C, indicating an intensification of micro-cracking due to heating and water cooling process. In some previous experimental studies (Wang et al. 2013), the thermal cracks density has been characterized in terms of crack porosity. The crack porosity was decreased by the increase of hydrostatic compressive stress due to the closure of thermal cracks. It is obvious that the crack porosity can be related to the residual strain investigated in the present work. The porosity is generally attributed to open cracks while the residual volumetric strain can also be attributed to closed cracks.

4.3 Evolution of gas permeability

The gas permeability evolution is a good indicator of cracking process induced by heating and water cooling process in granite samples. The gas permeability is inherently related to open microcracks. The gas permeability decrease in hydrostatic compression tests is a consequence of progressive closure of microcracks. Similar results have been obtained by Brace et al. (1968). The gas permeability increase is due to the creation of open microcracks by the heating-cooling treatment. Therefore, when the pre-treatment temperature is low, the density of microcracks due to heating-cooling process is small and the resulted gas permeability increase

is moderate. However, when the pre-treatment temperature is higher than 400^{o}C, there is a sudden increase of gas permeability due to thermal treatment while the magnitude of permeability decrease due to hydrostatic compression remains nearly the same as that for lower pre-treatment temperatures. The permeability evolution in thermally cracked rocks has also been investigated in some previous studies, for instance by Wang et al. (Wang et al. 2013). They have studied the permeability diminution with hydrostatic compression stress and both thermally cracked samples and intact ones. The heated samples were slowly cooled. They found that the permeability diminution rate varied from 0.06×10^{-16} m^2/MPa in damaged samples to 0.01×10^{-16} m^2/MPa in intact samples for the hydrostatic stress up to 30 MPa. In the present study on granite, as shown in Fig. 10, the permeability diminution rate is almost constant and equal to 0.8×10^{-18} m^2/MPa for tested samples. It is not easy to provide a definite explanation of this difference. One of reasons lies in the fact that the cooling procedure is different between two studies. In this paper, the heated samples are suddenly cooled in cold water down to room temperature. In Wang et al. (Wang et al. 2013), the heated samples were naturally cooled in the oven when the oven was turned off. It seems that the morphology of thermally induced cracks is influenced by the cooling procedure. On the other hand, the distribution of thermal induced cracks can also be related to initial microstructures of rocks. Therefore, further investigations are needed to fully capture the influence of cooling procedure on the process of thermal cracks.

5. Conclusions

In this paper, we have studied the evolutions of bulk compressibility and gas permeability in granite samples subjected to heating and rapid water cooling. Some including remarks can be drawn. The heating and water cooling process is responsible to microcracking in granite sample. The distribution of thermal microcracks can be related to mineralogical compositions and microstructures as well as sample geometry. In the case of cylindrical granite samples, more microcracks are oriented in the radial direction than in the axial direction. The oriented distribution of thermal microcracks affects the macroscopic mechanical properties of granite during subsequent loading. However, further microscopic investigations are still needed for a deep description og spatial distribution of thermal induced microcracks. The density of thermal microcracks increases when the pre-treatment temperature is higher. When the pre-treatment temperature is lower than 400°C, the density of thermal microcracks remains relatively small and most microcracks are closed under a hydrostatic compressive stress up to 50MPa. After that temperature, there is a significant increase of crack density. The majority of microcracks are not closed under a hydrostatic compressive stress up to 50MPa. The crack closure stress increases with the increasing of pre-treatment temperature. Therefore, for a given heating temperature, it will be possible to define a compressive stress threshold above that the heating-cooling process does not affect mechanical properties of granite. The residual volumetric strain after unloading is a good macroscopic indicator for quantifying thermally induced crack density in hard rocks as granite. As a consequence of thermally induced

cracking, there is a significant decrease of the initial elastic tangent bulk modulus of granite samples. At the same time, the gas permeability is increased by two orders of magnitude when the pre-treatment temperature reaches 900°C.

In future studies, it seems important to investigate effects of cooling method on the thermal cracking process by considering for instance gradual air cooling. Deeper studies are also necessary to better understand the transition in crystal structure of granite. The results obtained in the present paper, together with those found in previous and future studies, will help the design optimization of geothermal engineering with different in situ stresses and thermal conditions.

Acknowledgements:

This work was jointly supported by the Natural Science Foundation of China (grant numbers 51579093 and 51479193) as well as The State Key Basic Research Program of China (grant number 2015CB057905).

Accepted manuscript doi:
10.1680/jgeot.18.p.005

Notation

P_1	initial gas pressure
P_0	atmospheric pressure
ΔP_1	amount of gas pressure reduction
Δt	time interval
P_m	mean injection pressure
Q_m	mean volume flow rate
V_r	the volume of the buffer reservoir
$\Delta\rho$	the variation of the gas specific mass due to ΔP_1
K	overall permeability
μ	gas viscosity
S	cross-section of the sample
h	height of the sample
ε_v	volumetric strain
ε_a	axial strain
ε_r	radial strain
K_i	initial bulk modulus
σ_{10}	the hydrostatic stress corresponding to 10% of the final value of confining stress

Accepted manuscript doi:
10.1680/jgeot.18.p.005

ε_{10} the volumetric strain corresponding to 10% of the final value of confining stress

σ_0 the hydrostatic stress corresponding to the starting loading point

ε_0 the volumetric strain corresponding to the starting loading point

References:

Abbasi, M., P. Rostami, M. Keshavarz Moraveji and M. Sharifi (2017). "Generalized analytical solution for gravity drainage phenomena in finite matrix block with arbitrary time dependent inlet boundary condition and variable matrix block size." Journal of Petroleum Science and Engineering.

Beck, K., S. Janvier-Badosa, X. Brunetaud, Á. Török and M. Al-Mukhtar (2015). Non-destructive diagnosis by colorimetry of building stone subjected to high temperatures.

Berthomieu, G. and P. Jouanna (1984). "Stability of rock faces subjected to temperature changes—Application to hot dry granite." International Journal of Rock Mechanics and Mining Sciences & Geomechanics Abstracts **21**(5): 277-287.

Boukharov, G. N., M. W. Chanda and N. G. Boukharov (1995). "The three processes of brittle crystalline rock creep." International Journal of Rock Mechanics and Mining Sciences & Geomechanics Abstracts **32**(4): 325-335.

Brace, W. F., J. B. Walsh and W. T. Frangos (1968). "Permeability of granite under high pressure." J Geophs Res **73**(6): 2225-2236.

Brotóns, V., R. Tomás, S. Ivorra and J. C. Alarcón (2013). "Temperature influence on the physical and mechanical properties of a porous rock: San Julian's calcarenite." Engineering Geology **167**: 117-127.

Bruel, D. (2007). "Using the migration of the induced seismicity as a constraint for fractured Hot Dry Rock reservoir modelling." International Journal of Rock Mechanics & Mining Sciences **44**(8): 1106-1117.

Chaki, S., M. Takarli and W. P. Agbodjan (2008). "Influence of thermal damage on physical properties of a granite rock: Porosity, permeability and ultrasonic wave evolutions." Construction and Building Materials **22**(7): 1456-1461.

Chen, J. and F. Jiang (2015). "Designing multi-well layout for enhanced geothermal system to better exploit hot dry rock geothermal energy." Renewable Energy **74**: 37-48.

Chen, S., C. Yang and G. Wang (2017). "Evolution of thermal damage and permeability of Beishan granite." Applied Thermal Engineering **110**: 1533-1542.

Chen, Y.-L., J. Ni, W. Shao and R. Azzam (2012). "Experimental study on the influence of temperature on the mechanical properties of granite under uni-axial compression and fatigue loading." International Journal of Rock Mechanics and Mining Sciences **56**: 62-66.

David, C., B. Menéndez and M. Darot (1999). "Influence of stress-induced and thermal cracking on physical properties and microstructure of La Peyratte granite." International Journal of Rock Mechanics & Mining Sciences **36**(4): 433-448.

Fredrich, J. T. and T. F. Wong (1986). "Micromechanics of thermally induced cracking in three crustal rocks." Journal of Geophysical Research Solid Earth **91**(B12): 12743-12764.

Gaunt, H. E., P. R. Sammonds, P. G. Meredith and A. Chadderton (2016). "Effect of temperature on the permeability of lava dome rocks from the 2004-2008 eruption of Mount St. Helens." Bulletin of Volcanology **78**(4): 30.

Glover, P. W. J., P. Baud, M. Darot, P. G. Meredith, S. A. Boon, M. Leravalec, S. Zoussi and T. Reuschlé (1995). "α/β phase transition in quartz monitored using acoustic emissions." Geophysical Journal of the Royal Astronomical Society **120**(3): 775-782.

Gnatus, N. A. and M. D. Khutorskoy (2010). "Hot dry rocks: An inexhaustible and renewable source of energy." Lithology and Mineral Resources **45**(6): 593-600.

Griffiths, L., M. J. Heap, P. Baud and J. Schmittbuhl (2017). "Quantification of microcrack characteristics and implications for stiffness and strength of granite." International Journal of Rock Mechanics & Mining Sciences **100**(December 2017): 138-150.

Griffiths, L., Lengline, O., Heap, J., Baud, P., Schmittbuhl, J. (2018), Thermal microcracking in Westerly Granite using direct wave velocity, coda wave interferometry and acoustic emissions, Journal of Geophysical Research : Solid Earth 123 (3): 2246-2261.

Hajpál, M. and Á. Török (2004). "Mineralogical and colour changes of quartz sandstones by heat." Environmental Geology **46**(3): 311-322.

Heuze, F. E. (1983). "High-temperature mechanical, physical and Thermal properties of granitic rocks— A review." International Journal of Rock Mechanics and Mining Sciences & Geomechanics Abstracts **20**(1): 3-10.

Huang, Y.-H., S.-Q. Yang, W.-L. Tian, J. Zhao, D. Ma and C.-S. Zhang (2017). "Physical and mechanical behavior of granite containing pre-existing holes after high temperature treatment." Archives of Civil and Mechanical Engineering **17**(4): 912-925.

ISRM (1979). "Suggested methods for determining water content, porosity, density, absorption and related properties and swelling and slake-durability index properties : Part 2: Suggested methods for determining swelling and slake-durability index properties." International Journal of Rock Mechanics & Mining Science **16**(2): 151-156.

Kelkar, S., G. Woldegabriel and K. Rehfeldt (2015). "Lessons learned from the pioneering hot dry rock project at Fenton Hill, USA." Geothermics **63**: 5-14.

Kumari, W. G. P., P. G. Ranjith, M. S. A. Perera, B. K. Chen and I. M. Abdulagatov (2017). "Temperature-dependent mechanical behaviour of Australian Strathbogie granite with different cooling treatments." Engineering Geology **229**: 31-44.

Loosveldt, H., Z. Lafhaj and F. Skoczylas (2002). "Experimental study of gas and liquid permeability of a mortar." Cement & Concrete Research **32**(9): 1357-1363.

Mallet, C., J. Fortin, Y. Guéguen and F. Bouyer (2013). "Effective Elastic Properties of Cracked Solids: An Experimental Investigation." International Journal of Fracture 182(2): 275-282.

Mallet, C., J. Fortin, Y. Guéguen and F. Bouyer (2014). Sub-critical Crack Propagation in Glass in Reservoir Conditions. 76th EAGE Conference and Exhibition 2014.

Nasseri, M. H. B., B. S. A. Tatone, G. Grasselli and R. P. Young (2009). "Fracture Toughness and Fracture Roughness Interrelationship in Thermally treated Westerly Granite." Pure and Applied Geophysics **166**(5): 801-822.

Ougier-Simonin, A., J. Fortin, Y. Guéguen, A. Schubnel and F. Bouyer (2011). "Cracks in glass under triaxial conditions." International Journal of Engineering Science 49(1): 105-121.

Ougier‐Simonin, A., Y. Guéguen, J. Fortin, A. Schubnel and F. Bouyer (2011). "Permeability and elastic properties of cracked glass under pressure." Journal of Geophysical Research: Solid Earth 116(B7).

Pei, L., G. Blöcher, H. Milsch, F. Deon, G. Zimmermann, W. Rühaak, I. Sass and E. Huenges (2016). "Thermal strain in a water-saturated limestone under hydrostatic and deviatoric stress states." Tectonophysics **688**: 49-64.

Shao, S., P. G. Ranjith, P. L. P. Wasantha and B. K. Chen (2015). "Experimental and numerical studies on the mechanical behaviour of Australian Strathbogie granite at high temperatures: An application to geothermal energy." Geothermics **54**: 96-108.

Shao, S., P. L. P. Wasantha, P. G. Ranjith and B. K. Chen (2014). "Effect of cooling rate on the mechanical behavior of heated Strathbogie granite with different grain sizes." International Journal of Rock Mechanics and Mining Sciences **70**: 381-387.

Takarli, M., W. Prince and R. Siddique (2008). "Damage in granite under heating/cooling cycles and water freeze–thaw condition." International Journal of Rock Mechanics and Mining Sciences **45**(7): 1164-1175.

Tian, H., T. Kempka, S. Yu and M. Ziegler (2016). "Mechanical Properties of Sandstones Exposed to High Temperature." Rock Mechanics and Rock Engineering **49**(1): 321-327.

Tomac, I. and M. Sauter (2017). "A review on challenges in the assessment of geomechanical rock performance for deep geothermal reservoir development." Renewable & Sustainable Energy Reviews **82**.

Vinciguerra, S., C. Trovato, P. G. Meredith and P. M. Benson (2005). "Relating seismic velocities, thermal cracking and permeability in Mt. Etna and Iceland basalts." International Journal of Rock Mechanics & Mining Sciences **42**(7–8): 900-910.

Vinciguerra, S., C. Trovato, P. G. Meredith and P. M. Benson (2005). "Relating seismic velocities, thermal cracking and permeability in Mt. Etna and Iceland basalts." International Journal of Rock Mechanics and Mining Sciences **42**(7): 900-910.

Violay, M., M. J. Heap, M. Acosta and C. Madonna (2017). "Porosity evolution at the brittle-ductile transition in the continental crust: Implications for deep hydro-geothermal circulation." Scientific Reports **7**(1).

Wang, X. Q., A. Schubnel, J. Fortin, Y. Guéguen and H. K. Ge (2013). "Physical properties and brittle strength of thermally cracked granite under confinement." Journal of Geophysical Research: Solid Earth 118(12): 6099-6112.

Wnuk, M. P. (1982). EFFECTS OF SIZE AND GEOMETRY ON STABILITY OF A GEOTHERMAL RESERVOIR CONTAINED BY HOT DRY ROCK A2 - Yuan, S.W. Energy, Resources and Environment, Pergamon**:** 308-315.

Wong T.F., 1982. Micromechanics of faulting in Westerly granite. Int. J. Rock Mech. Min. Sci. 19, 49-62

Yang, S.-Q., P. G. Ranjith, H.-W. Jing, W.-L. Tian and Y. Ju (2017). "An experimental investigation on thermal damage and failure mechanical behavior of granite after exposure to different high temperature treatments." Geothermics **65**: 180-197.

Yavuz, H., S. Demirdag and S. Caran (2010). "Thermal effect on the physical properties of carbonate rocks." International Journal of Rock Mechanics and Mining Sciences **47**(1): 94-103.

Yong, C. and C. Y. Wang (1980). "Thermally induced acoustic emission in westerly granite." Geophysical Research Letters **7**(12): 1089-1092.

Zeng, Y.-C., Z. Su and N.-Y. Wu (2013). "Numerical simulation of heat production potential from hot dry rock by water circulating through two horizontal wells at Desert Peak geothermal field." Energy **56**: 92-107.

Zhang, F., J.J. Zhao, D. Hu, F. Skoczylas and J.F. Shao (2018). "Laboratory investigation on physical and mechanical properties of granite after heating and water-cooling treatment", Rock Mechanics and Rock Engineering **51**(3): 677-694.

Zhang, L., X. Mao and A. Lu (2009). "Experimental study on the mechanical properties of rocks at high temperature." Science in China Series E: Technological Sciences **52**(3): 641-646.

Zhao, Y., Z. Feng, B. Xi, Z. Wan, D. Yang and W. Liang (2015). "Deformation and instability failure of borehole at high temperature and high pressure in Hot Dry Rock exploitation." Renewable Energy **77**: 159-165.

Zhao, Z. (2016). "Thermal Influence on Mechanical Properties of Granite: A Microcracking Perspective." Rock Mechanics and Rock Engineering **49**(3): 747-762.

Zheng, Q., T. Shimizu and M. Yang (2017). "Grain size effect on mechanical behavior of thin pure titanium foils at elevated temperatures." International Journal of Mechanical Sciences **133**: 416-425.

Zhu QZ, Zhao LY, Shao JF (2016), Analytical and numerical analysis of frictional damage in quasi brittle materials, Journal of the Mechanics and Physics of Solids 92 (2016): 137-163

Accepted manuscript doi:
10.1680/jgeot.18.p.005

Table 1: Initial tangent modulus, crack closure stress and strain, residual strain versus pre-treatment temperature

Heating Temperature (°C)	Initial tangent bulk modulus (MPa)	Crack closure stress (MPa)	Crack closure strain (%)	Residual strain (%)
25	3699.36±90.84	34±1.63	0.625±0.08	0.29±0.03
200	2089.17±134.54	35±1.25	0.80±0.02	0.42±0.05
300	1048.04±75.12	37±2.50	1.24±0.03	0.78±0.11
400	856.76±59.92	37±1.00	1.75±0.05	1.12±0.23
500	420.85±43.30	45±2.50	2.75±0.16	2.30±0.22
600	294.69±66.49	46±2.02	4.40±0.18	3.92±0.42
900	283.76±6.93	48±5.03	5.20±0.45	4.70±0.34

Accepted manuscript doi:
10.1680/jgeot.18.p.005

Caption of Figures:

Fig. 1 Thermo-hydro-mechanical-chemical coupling testing system
Fig. 2 Sketch of gas permeability apparatus
Fig. 3 Color evolution of granite samples after heating and water-cooled treatment
Fig. 4 Polarized light microscopy images
Fig4a: Intact sample
Fig4b: Damaged sample for 900^{o}C
Fig. 5 Growth of microcracks at different values of pre-treatment temperature
Fig5a: T=20°C
Fig5b: T=200°C
Fig5c: T=300°C
Fig5d: T=400°C
Fig5e: T=500°C
Fig5e: T=600°C
Fig5g: T=900°C

Fig. 6. Typical stress-strain curves in hydrostatic compression tests for different levels of pre-treatment temperature and illustration of initial bulk modulus identification (Fig. 5a)
Fig6a: T=20°C
Fig6b: T=200°C
Fig6c: T=300°C
Fig6d: T=400°C
Fig6e: T=500°C
Fig6e: T=600°C
Fig6g: T=900°C

Fig. 7 Variations of initial tangent bulk modulus and residual strain with pre-treatment temperature

Fig. 8 Volumetric strain versus hydrostatic stress and determination of residual strain

Fig. 9 Crack closure stress and strain for different values of pre-treatment temperature

Fig. 10 Evolutions of gas permeability with hydrostatic stress

Fig. 11 Evolutions of gas permeability with pre-treatment temperature

Accepted manuscript doi:
10.1680/jgeot.18.p.005

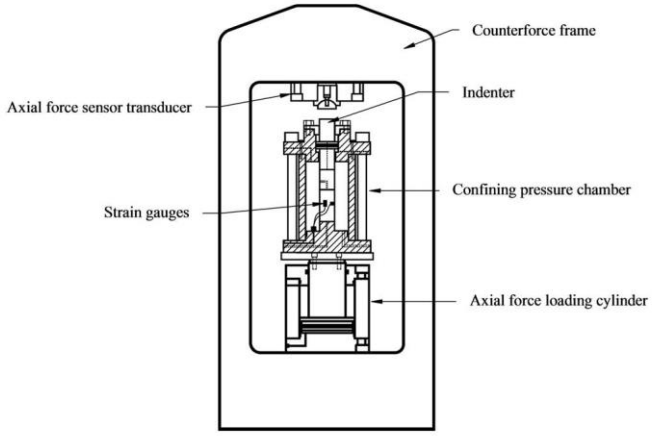

Fig.1

Accepted manuscript doi:
10.1680/jgeot.18.p.005

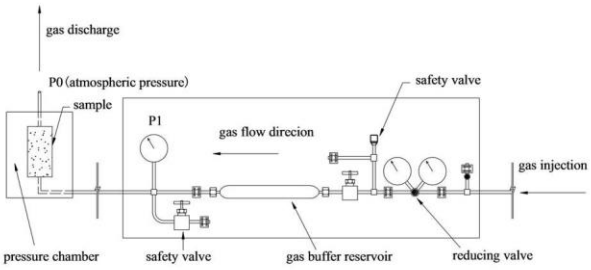

Fig.2

Accepted manuscript doi:
10.1680/jgeot.18.p.005

Fig.3

Accepted manuscript doi:
10.1680/jgeot.18.p.005

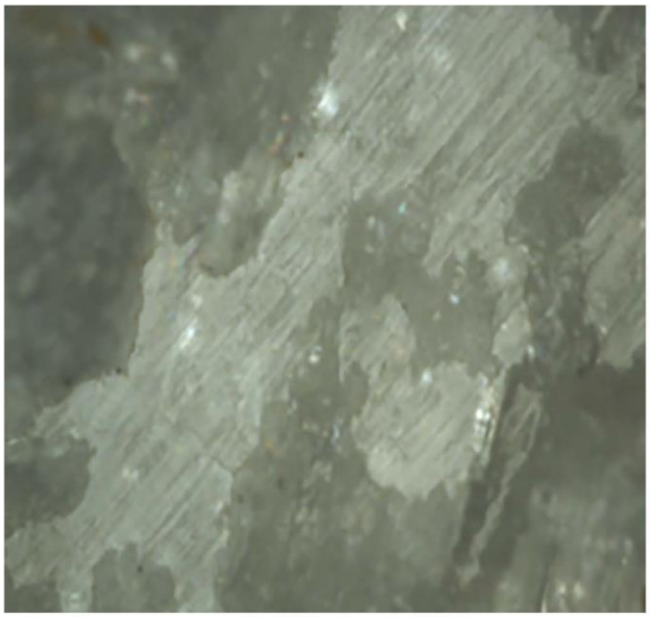

Fig.4(a)

Accepted manuscript doi:
10.1680/jgeot.18.p.005

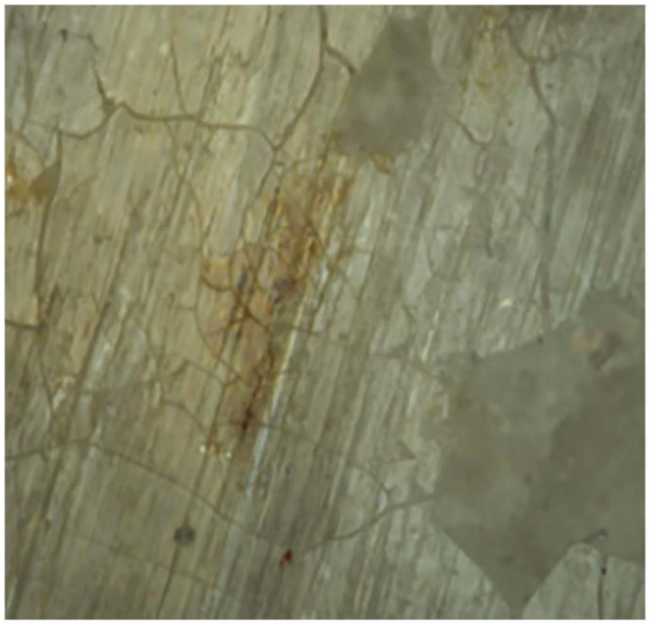

Fig.4(b)

Accepted manuscript doi:
10.1680/jgeot.18.p.005

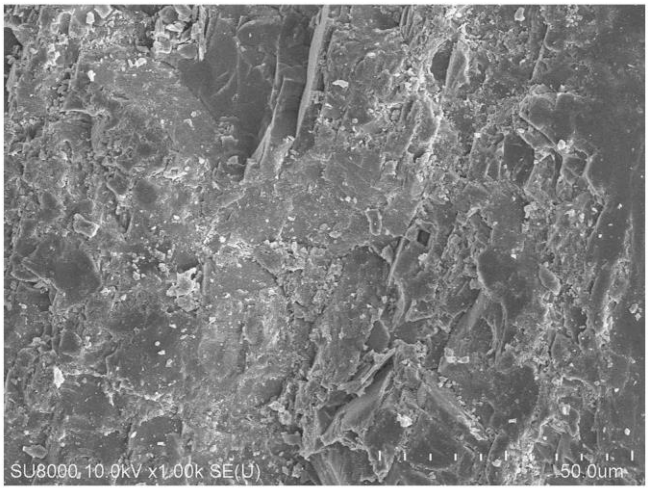

Fig.5(a)

Accepted manuscript doi:
10.1680/jgeot.18.p.005

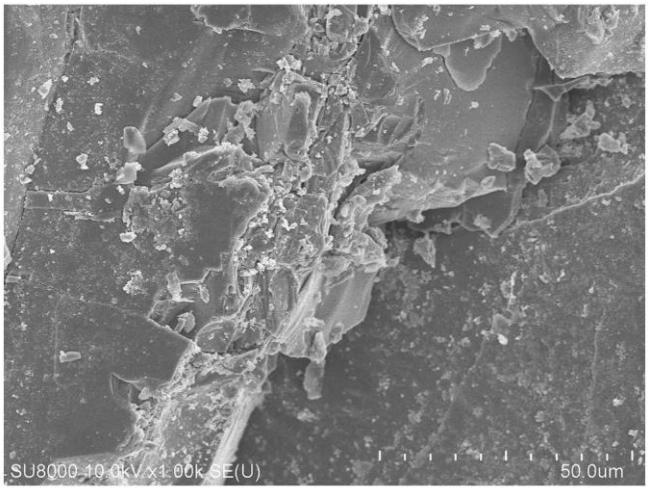

Fig.5(b)

Accepted manuscript doi:
10.1680/jgeot.18.p.005

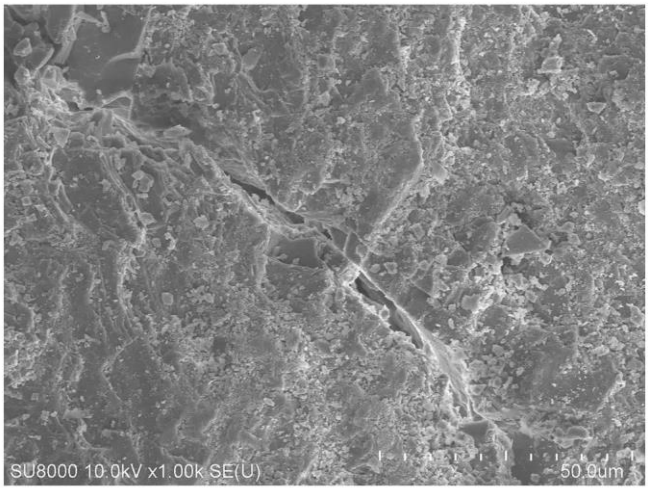

Fig.5(c)

Accepted manuscript doi:
10.1680/jgeot.18.p.005

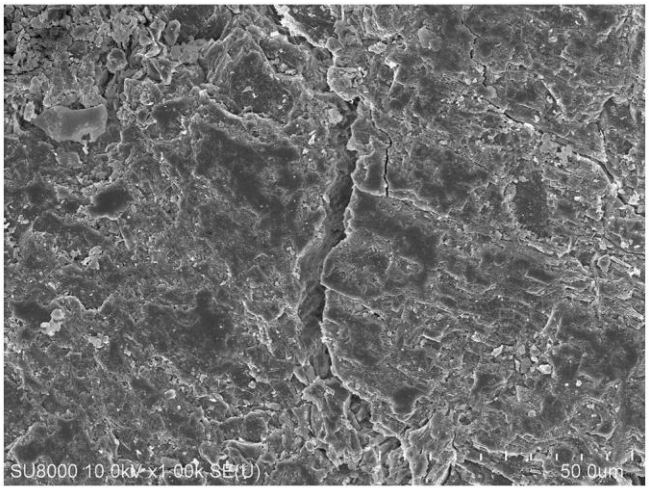

Fig.5(d)

Accepted manuscript doi:
10.1680/jgeot.18.p.005

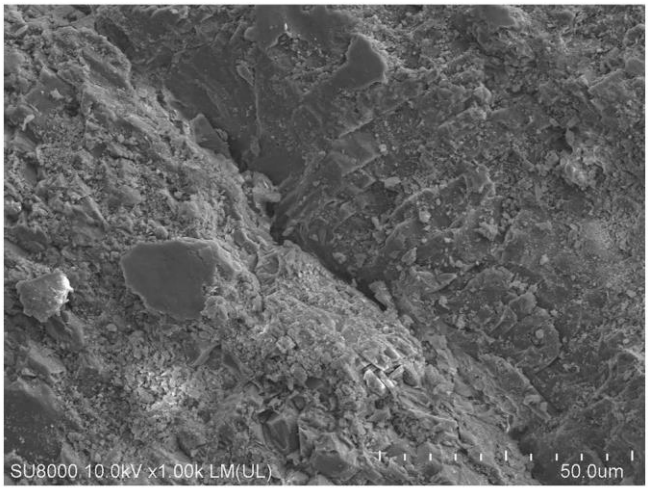

Fig.5(e)

Accepted manuscript doi:
10.1680/jgeot.18.p.005

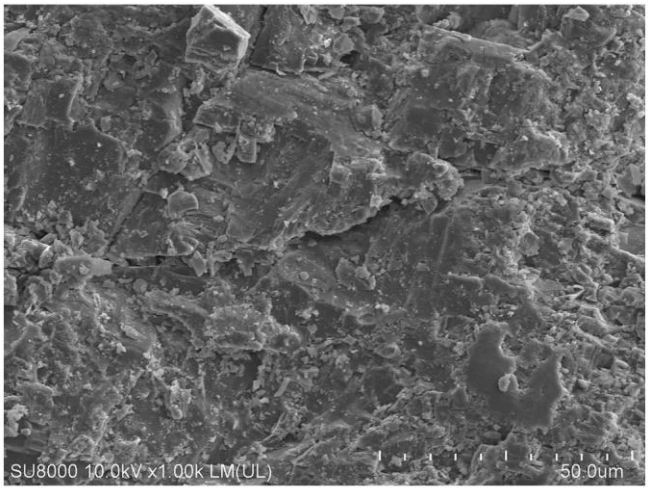

Fig.5(f)

Accepted manuscript doi:
10.1680/jgeot.18.p.005

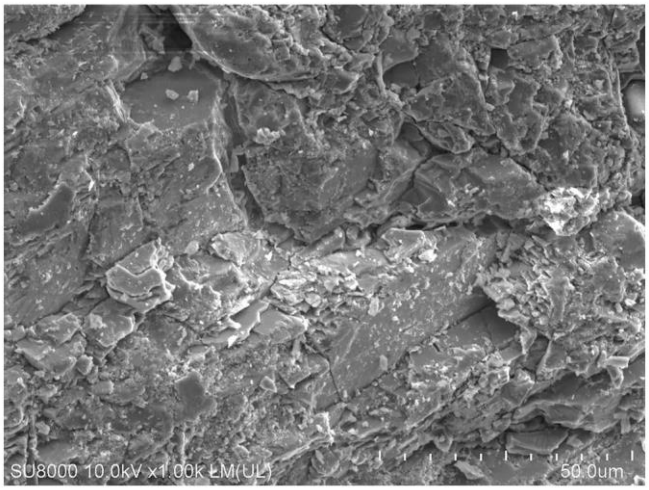

Fig.5(g)

Accepted manuscript doi:
10.1680/jgeot.18.p.005

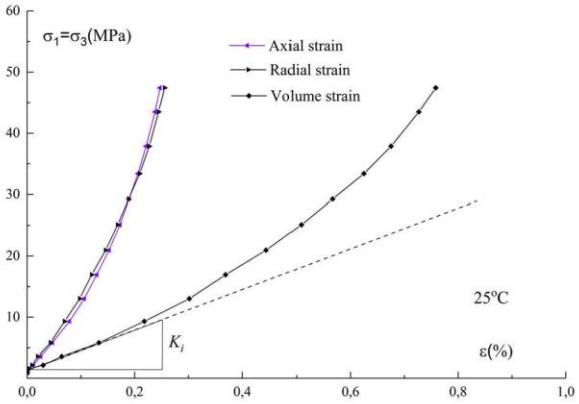

Fig.6(a)

Accepted manuscript doi:
10.1680/jgeot.18.p.005

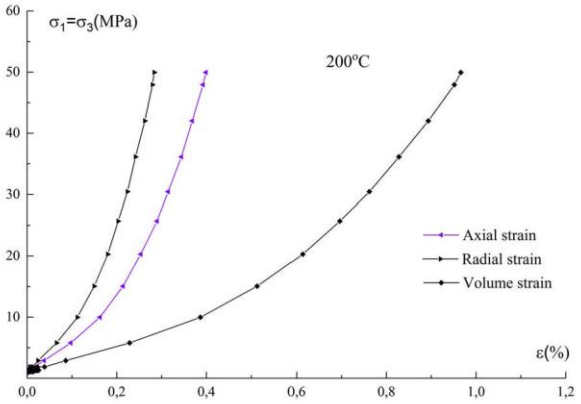

Fig.6(b)

Accepted manuscript doi:
10.1680/jgeot.18.p.005

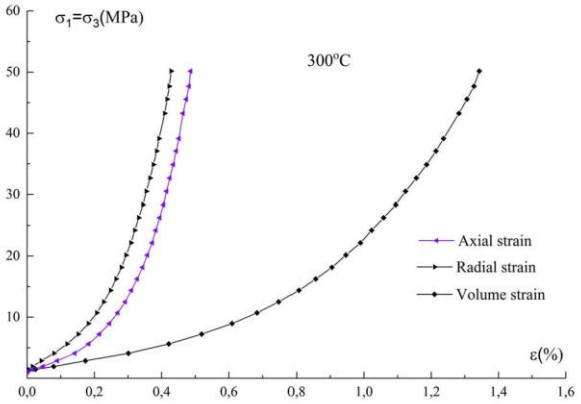

Fig.6(c)

Accepted manuscript doi:
10.1680/jgeot.18.p.005

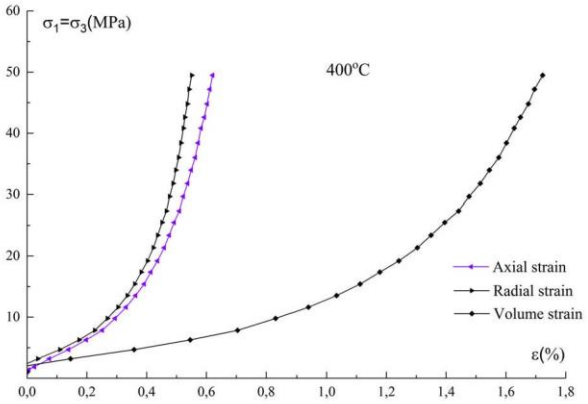

Fig.6(d)

Accepted manuscript doi:
10.1680/jgeot.18.p.005

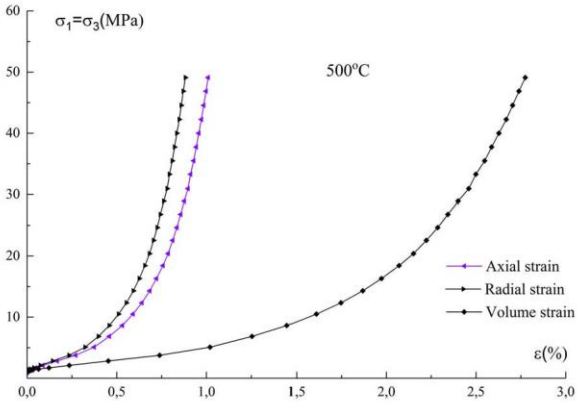

Fig.6(e)

Accepted manuscript doi:
10.1680/jgeot.18.p.005

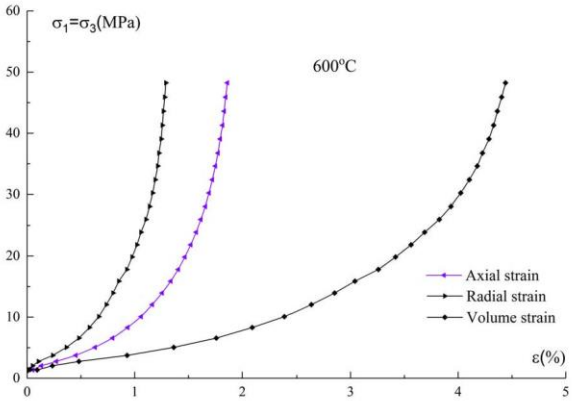

Fig.6(f)

Accepted manuscript doi:
10.1680/jgeot.18.p.005

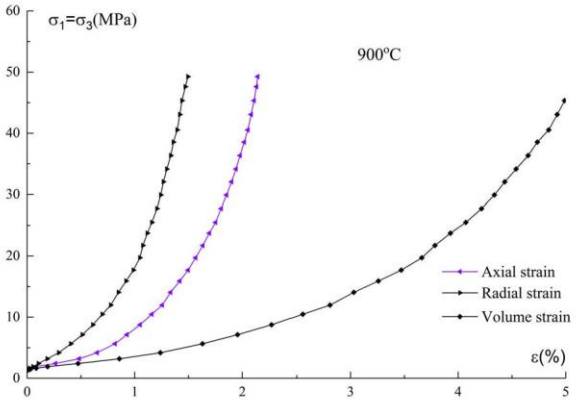

Fig.6(g)

Accepted manuscript doi:
10.1680/jgeot.18.p.005

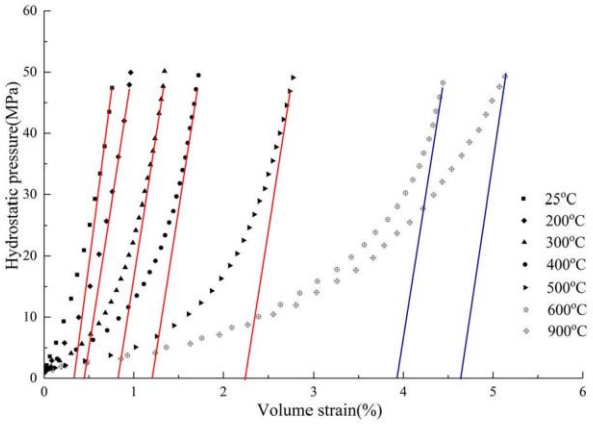

Fig.7

Accepted manuscript doi:
10.1680/jgeot.18.p.005

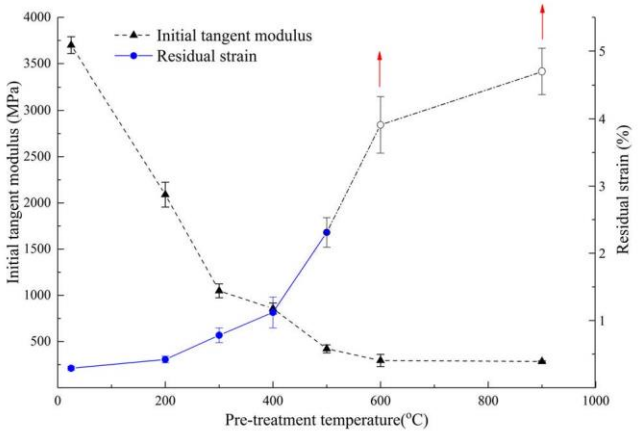

Fig.8

Accepted manuscript doi:
10.1680/jgeot.18.p.005

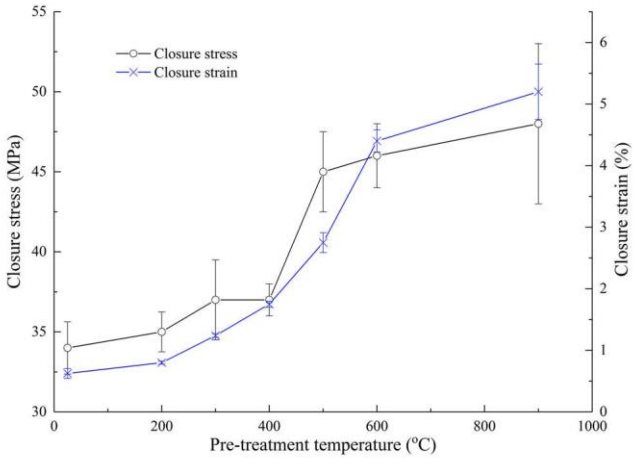

Fig.9

Accepted manuscript doi:
10.1680/jgeot.18.p.005

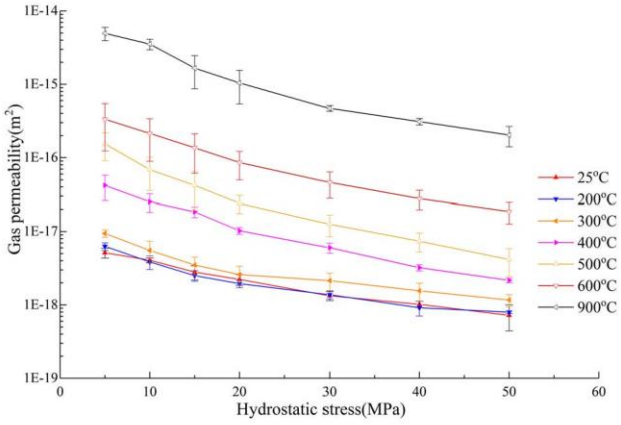

Fig.10

Accepted manuscript doi:
10.1680/jgeot.18.p.005

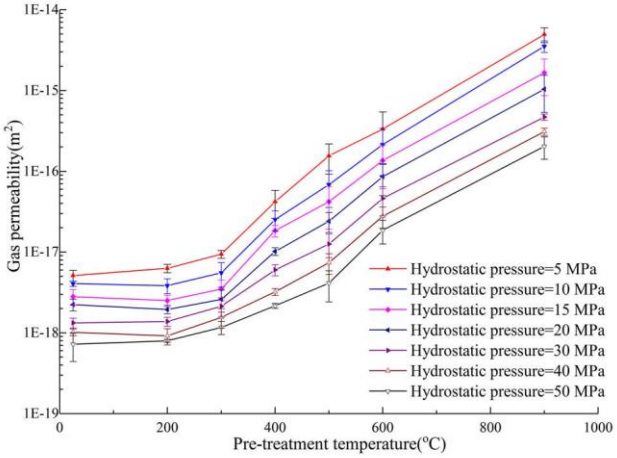

Fig.11